Chemistry
A European
Journal

Chemistry Europe
European Chemical Societies Publishing

Accepted Article

Title: Deconvolving Contributions to Decoherence in Molecular Electron Spin Qubits: A Dynamic Ligand Field Approach

Authors: Ruben Mirzoyan, Nathanael P. Kazmierczak, and Ryan G. Hadt

To be cited as: *Chem. Eur. J.* 10.1002/chem.202100845

Link to VoR: https://doi.org/10.1002/chem.202100845

WILEY-VCH

10.1002/chem.202100845

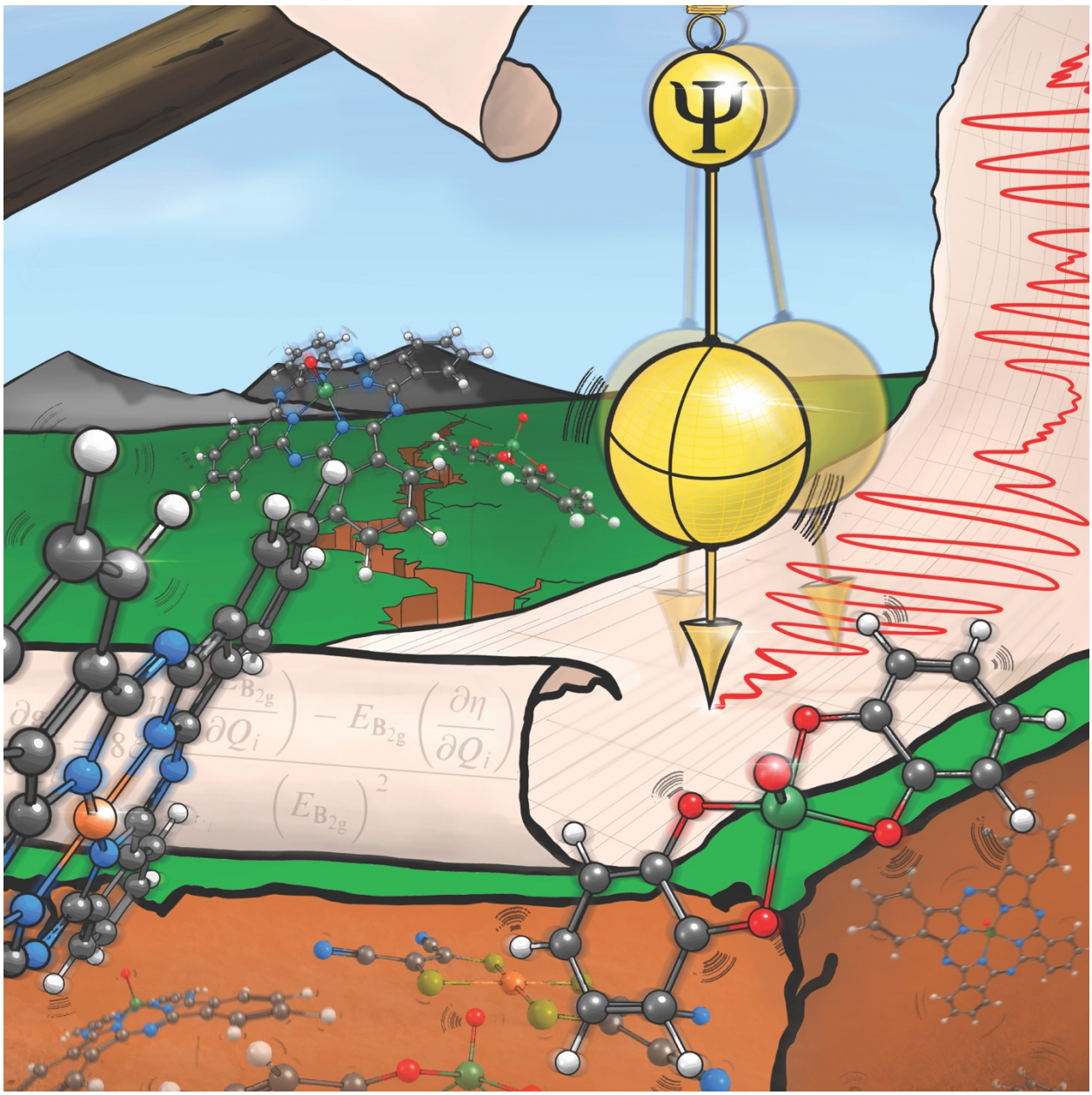

10.1002/chem.202100845

Deconvolving Contributions to Decoherence in Molecular Electron Spin Qubits: A Dynamic Ligand Field Approach

Ruben Mirzoyan, Nathanael P. Kazmierczak, and Prof. Ryan G. Hadt*

Division of Chemistry and Chemical Engineering, Arthur Amos Noyes Laboratory of Chemical Physics, California Institute of Technology, Pasadena, CA 91125, United States

*Corresponding Author: rghadt@caltech.edu

Abstract

In the past decade, transition metal complexes have gained momentum as electron spin-based quantum bit (qubit) candidates due to their synthetic tunability and long achievable coherence times. The decoherence of magnetic quantum states imposes a limit on the use of these qubits for quantum information technologies, such as quantum computing, sensing, and communication. With rapid recent development in the field of molecular quantum information science, a variety of chemical design principles for prolonging coherence in molecular transition metal qubits have been proposed. Here we delineate the spin-spin, motional, and spin-phonon regimes of decoherence, outlining design principles for each. We show how dynamic ligand field models can provide insights into the intramolecular vibrational contributions in the spin-phonon decoherence regime. This minireview aims to inform the development of molecular quantum technologies tailored for different environments and conditions.

Introduction

Motivation

Near the beginning of the 20th century, quantum mechanics developed new fundamental rules that describe the natural world, constituting the first quantum revolution. The second quantum revolution now endeavors to control individual quantum systems, enabling powerful applications in computing, sensing, and communication.[1,2] The fundamental unit of quantum information science is the quantum bit (qubit), a two-level quantum system.[3] Paramagnetic molecules can serve as qubit platforms due to the Zeeman effect, wherein the M_S sublevels of an unpaired electron in a magnetic field generate an effective two-level system with an energy gap in the microwave frequency range (Figure 1A). The quantum states of electron spins can then be initialized, manipulated, and studied using microwave pulses in electron paramagnetic resonance (EPR) spectrometers.[4] Furthermore, paramagnetic transition metal complexes are synthetically tunable and can be attached to templated substrates and surfaces,[5] tethered to electrodes,[6] and integrated with superconducting resonators[7,8] to realize quantum technological devices tunable on the molecular scale.[9–15]

Defining and Using Quantum Coherence

An essential feature of quantum systems is the property of phase coherence (hereafter simply "coherence"), in which qubits in an ensemble retain their relative phase relations.[16] Interactions between the qubits and their environment cause the ensemble to lose coherence and collapse to a classically observable state, limiting the time in which uniquely quantum behavior can be observed. This process is known as decoherence.[16] Successful electron spin qubits in both sensing and computing must have long coherence times relative to their Larmor precession frequency,

which governs the limiting timescale at which the electron spin qubit can change its quantum state. Using X-band EPR (~9.5 GHz), this timescale is on the order of 10 ns. To maintain phase information adequate for fault-tolerant quantum computations, the coherence time should be 10^4–10^5 times longer.[17] Therefore, understanding the contributions to coherence times is a critical factor for the development of technologies that exploit quantum information.[2]

In the simplest model, decoherence of an S = ½ system can be described by two mono-exponential processes, with time constants T_1 and T_2 based on the Bloch equations.[18] T_1 defines the time required for an ensemble of electron spins to relax back to thermodynamic equilibrium, a criterion satisfied when the Zeeman-split magnetic sublevels are populated according to a Boltzmann distribution. For an initial excess of excited spins, this requires dissipation of energy to a surrounding bath or lattice. T_1 is therefore often called the "spin-lattice" relaxation time, though the environment need not necessarily be a crystalline lattice. T_2 defines the time required for an ensemble of spins to lose their phase relations. This does not necessitate dissipation of energy to the lattice and arises from the differential couplings between qubit electron spins and spins in the bath. For this reason, T_2 is often called the "spin-spin" relaxation time. Both processes can be visualized by considering spin magnetization vectors projected onto a complex unit sphere known as the Bloch sphere (Figure 1A). A pure (coherent) state is represented by a vector extending towards a point on the surface of the sphere, while a mixed (partially or fully decohered) state is representing by a vector extending towards a point within the interior of the sphere.[3] As can be seen geometrically, longitudinal electron spin relaxation (T_1) necessarily destroys transverse magnetization (Figure 1B). Therefore, the upper limit to T_2 (Figure 1C) is defined by T_1, in which case T_2 is said to be T_1-limited. This regime is important to consider when seeking to increase the temperature at which coherence can be maintained and used.

10.1002/chem.202100845

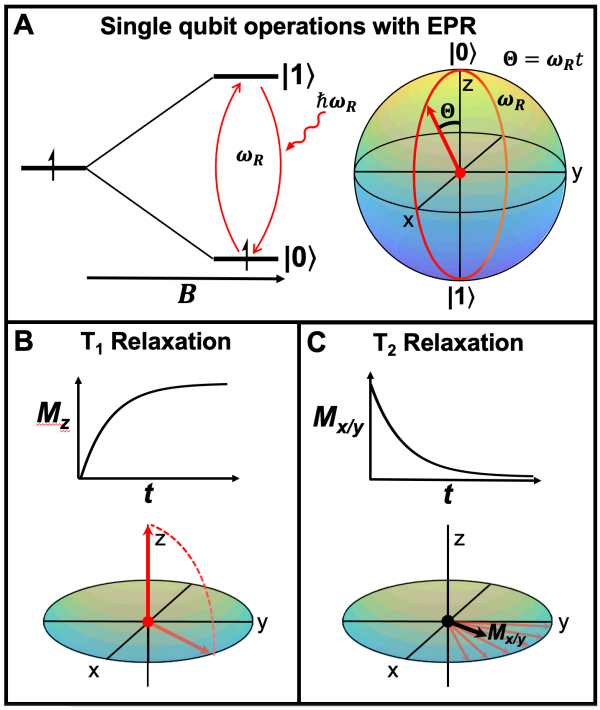

Figure 1. *Principles of qubit measurements in EPR spectroscopy.* ***(A)*** *Magnetically split electron spin sublevels serve as the qubit platform. The quantum state can be controlled by the microwave pulse length t, which alters the wavefunction parameter* Θ *in the Bloch sphere representation of the single qubit.* ***(B)*** T_1 *relaxation, as depicted by the recovery of net longitudinal magnetization* $\boldsymbol{M_z}$ *in the rotating frame representation.* ***(C)*** T_2 *relaxation, as depicted by the decrease in the net transverse magnetization vector* $\boldsymbol{M_{x/y}}$ *(black arrow) as the ensemble of spins (red arrows) lose their phase coherence. The* T_1 *contribution to* T_2 *is not shown.*

The characteristic decoherence time constants can be determined experimentally using pulsed EPR spectroscopy. An initial state is prepared by a coherent pulse, which both excites members of the spin ensemble and synchronizes their phases. Experimental coherence times are defined herein by time constants T_2^{DD}, T_M, and T_2^*; each pertains to a time decay following a well-defined pulse sequence (Figure 2A). It should be noted that naming convention can differ, and

10.1002/chem.202100845

some authors refer to T_2 and T_M interchangeably. T_2^* corresponds to the free-induction decay following a single $\pi/2$ pulse and is the simplest measurement of decoherence. T_M corresponds to the decay following a Hahn-echo pulse sequence, in which a π pulse removes dephasing due to static inhomogeneities in the magnetic environment (Figure 2B). T_2 as defined by Bloch cannot usually be measured in EPR owing to spectral diffusion (Figure 2C),[19] a process arising from the narrow bandwidth of the microwave radiation compared to the absorbance lineshape. In some cases, dynamic decoupling methods can more closely measure T_2 by filtering out quantum noise at the frequency corresponding to the interactions (typically hyperfine) that dominate spectral diffusion. The commonly used Carr-Purcell-Meiboom-Gill (CPMG) pulse sequence uses a train of "rephasing" π pulses, which can substantially diminish spectral diffusion effects in EPR dephasing.[20–22] While dynamical decoupling methods are powerful, the upper limit for coherence times are set by the molecular properties of the qubit. Thus, this minireview focuses on establishing design principles for long quantum coherence times through synthetically tunable chemical properties of the qubit and its environment.

10.1002/chem.202100845

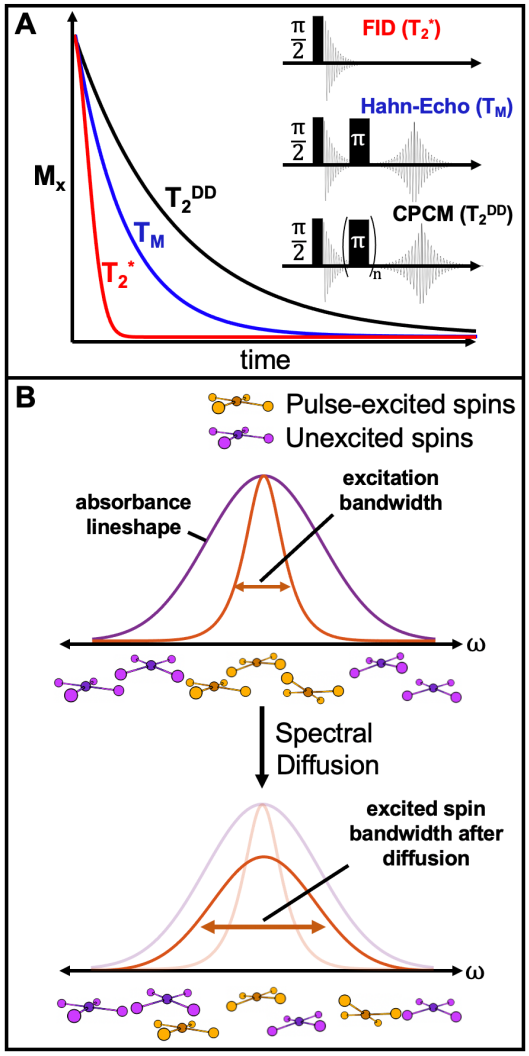

Figure 2. *Experimental methods and considerations for spin coherence.* ***(A)*** *Overlay of FID (T_2*), Hahn-echo (T_M), and dynamically decoupled echo (T_2^{DD}) decays, together with the corresponding pulse sequences to measure these time constants.* ***(B)*** *Schematic illustration of spectral diffusion, in which magnetic interactions modify the resonant frequency of excited spins after excitation.*

The Idea of Decoherence Regimes

To understand factors leading to decoherence, it is useful to consider the terms of the spin Hamiltonian for the transition metal complex. A common model for decoherence is based on a quantum bath approach, in which the qubit and the bath are together considered as a closed

quantum system.[23] The Hamiltonian of the system is defined as $\boldsymbol{H} = \boldsymbol{H}_{\mathrm{spin}} + \boldsymbol{H}_{\mathrm{bath}} + \boldsymbol{H}_{\mathrm{int}}$, where the spin Hamiltonian $\boldsymbol{H}_{\mathrm{spin}}$ for a transition metal complex is given by:

$$\boldsymbol{H}_{\mathrm{spin}} = \mu_e \boldsymbol{g}\hat{\boldsymbol{S}}\boldsymbol{B_0} + \hat{\boldsymbol{S}}\boldsymbol{A}\hat{\boldsymbol{I}} + \hat{\boldsymbol{S}}\boldsymbol{D}\hat{\boldsymbol{S}} \quad (1)$$

In order of appearance, Equation 1 contains the electronic Zeeman, hyperfine, and zero-field splitting terms. Here the external magnetic field is $\boldsymbol{B_0}$ and the electron and nuclear spin angular momenta are $\hat{\boldsymbol{S}}$ and $\hat{\boldsymbol{I}}$, with hyperfine tensor $\boldsymbol{A}$ and electronic g-tensor $\boldsymbol{g}$. The zero-field splitting tensor is given by $\boldsymbol{D}$ and is considered for systems in which the total electron spin is S > ½. The spin-bath interaction term $\boldsymbol{H}_{\mathrm{int}}$ determines the decoherence properties of any molecular electron spin qubit.

A variety of strategies for increasing coherence times have been pursued, leading to different design principles for different goals and conditions. To prolong T_M, much emphasis has been placed on suppressing hyperfine interactions through nuclear spin dilution,[24–27] elimination,[28] substitution with nuclei having smaller magnetic moments,[27,29,30] and, more recently, "patterning",[31] in which the neighboring nuclei of a lattice or ligand framework have a mismatch in their magnetic moments. These strategies suppress dipolar and hyperfine interaction terms in $\boldsymbol{H}_{\mathrm{int}}$. The current record for the longest T_M in a transition metal complex is 0.7 ms at 10 K, which was observed for a six-coordinate V(IV) complex having a nuclear spin-free ligand and solvent environment (CS_2).[28] Inspired from atomic physics, another approach uses clock transitions, in which the Zeeman energy is centered at an avoided level crossing to suppress magnetic noise.[32–35] To prolong T_1, several studies have chosen structurally rigid ligand frameworks that suppress the effect of molecular vibrations and their modulation of spin-orbit coupling, with specific emphasis on building around the vanadyl (VO) moiety.[36–38] A recent strategy has targeted the minimization of ground state orbital angular momentum in a series of 3d

10.1002/chem.202100845

and 4f metal complexes.[39] Despite possessing concentrated nuclear spins and a ligand framework that is structurally non-rigid, the isotropic ground state wave function enabled these qubits to reach µs coherence times at room temperature. To enable applications, molecular design is often inspired from a desired initialization or readout mechanism of the quantum state. For instance, optically addressable S = 1 molecular qubits, such as recently synthesized Cr(IV) complexes,[40] feature a spin-selective intersystem crossing in the excited state that enables a fluorescence-based readout of the quantum state. Such readout mechanisms were inspired[41] by the famous optically addressable solid-state electron spin qubits, such as nitrogen vacancy centers in diamond[42,43] and the divacancies in the 4H polytype of silicon carbide.[44] Alternatively, single qubit control may be pursued through the spatial resolution offered by metal organic frameworks (MOFs).[45,46] In accordance with the variety of experimental goals and design strategies, molecular qubit candidates display substantial structural diversity (Figure 3). Care must be taken to determine the dominant processes responsible for decoherence under a given set of conditions.

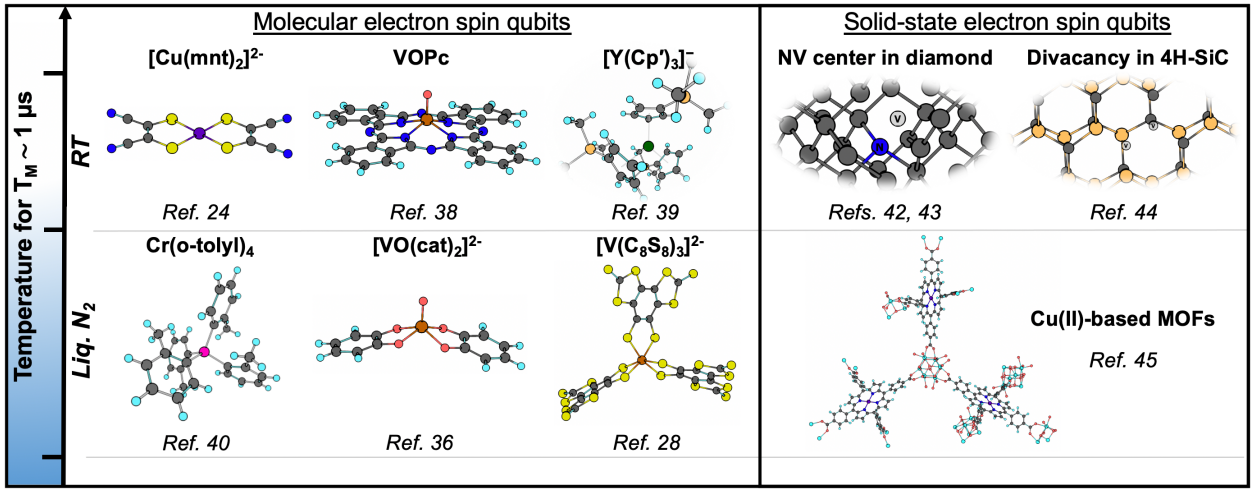

Figure 3. *Representative electronic spin-based qubits.*[24,28,36,38–40,42,44,45] *Top row: representative qubits exceeding T_M = 1 µs at room temperature. Abbreviations: (mnt) = maleonitriledithiolate; VOPc = vanadyl phthalocyanine; Cp' = ($C_5H_4SiMe_3$); (cat) = catecholate. Atomic Color Scheme:*

10.1002/chem.202100845

Cu (purple), S (yellow), C (charcoal gray), V (orange), Cr (pink), O (red), N (blue), Si (dark yellow), H (cyan), Y (dark green).

The dominant decoherence processes of molecular qubits can be categorized into three distinct regimes: the spin-spin (Figure 4A), motional (Figure 4B), and spin-phonon limits (Figure 4C). In the spin-spin regime, the spin bath dominates T_M through electronic and nuclear spin flip-flops. In the motional limit, T_M is dominated by molecular tumbling (solution phase) or low amplitude librations (glassy solids), which dynamically change the portion of the anisotropic Zeeman tensor aligned with the external magnetic field. In the spin-phonon limit, T_M is limited by T_1, which is dominated by intramolecular vibrations that modulate the orbital angular momentum of the ground state. Each of the three regimes will be discussed in turn.

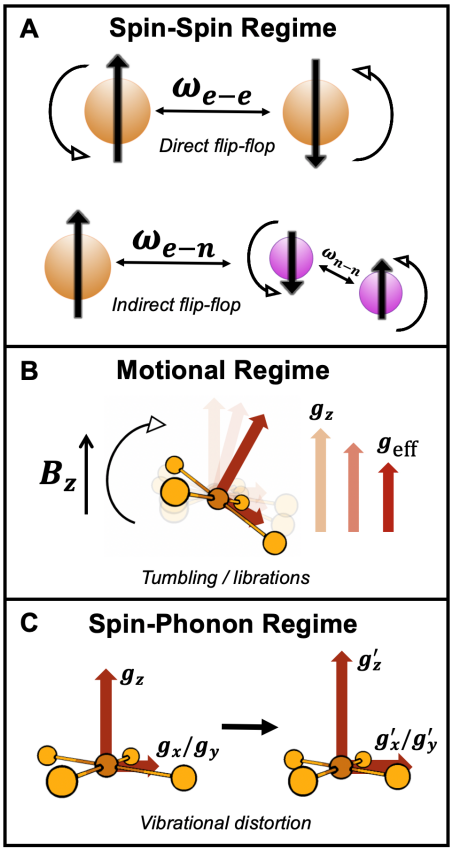

Figure 4. *Regimes of decoherence in molecular electron spin qubits.* ***(A)*** *Dipolar flip-flops dominate the spin-spin decoherence regime, which occurs at low temperatures and in concentrated spin environments. Direct flip-flops occur when a pair of spins exchanges their spin angular momenta, while indirect flip-flops arise from interaction with nearby spin pairs.* ***(B)*** *Tumbling and librational dynamics characterize the motional decoherence regime, which occurs in liquids and glassy solids containing molecules with anisotropic Zeeman or hyperfine tensors.* ***(C)*** *Vibrationally-induced molecular distortions characterize the spin-phonon decoherence regime, which dominates at high temperatures in the solid phase.*

Spin-Spin and Motional Contributions to Decoherence

Electron spin qubits undergo decoherence in the presence of other electronic and nuclear spins in the environment due to the coupling of spin angular momenta. Electron and nuclear spins both on the qubit molecule and within the bath can undergo thermal energy-conserving flip-flops, which perturb the magnetic dipolar coupling of the electron spin qubit and induce decoherence.[47] Direct and indirect spin-spin interactions contributing to T_M are represented in Figure 4A. Spin-spin decoherence arises primarily through hyperfine coupling with nuclear spins in the solvent,[26,28] hyperfine coupling with nuclear spins on the ligands,[48] and direct spin flip-flops between electronic spin centers.[45,46] To minimize the latter contribution, dilution of the paramagnetic qubit in a matrix of a diamagnetic analog is a commonly employed strategy.[49] The suppression of hyperfine coupling is attained through nuclear-spin-free ligand scaffolds and spin-free solvents, such as carbon disulfide, which have shown great success.[28]

An additional key consideration is the spin-diffusion barrier,[50,51] in which nuclear spins that are within a 4–8 Å radius of the electron spin contribute only a small degree to decoherence.[52]

10.1002/chem.202100845

Nuclei within the barrier couple strongly to the electron spin, which detunes them to other nuclei in the bath, reducing their participation in nuclear spin flip-flops. Experimental evidence for the spin-diffusion barrier has been obtained from a series of vanadyl complexes using carbon/sulfur ligand scaffolds to systematically vary the distance between the terminal hydrogens and the electron spin center.[53] Molecules containing hydrogen atoms only within 6 Å were found to have a sharp increase in coherence time, owing to strengthened coupling between the hydrogen-based nuclear spins and the vanadium-based unpaired electron. Some models for fitting T_2 data have incorporated the spin diffusion barrier radius.[26,54–56]

Additional decoherence mechanisms are possible whenever an electron spin qubit exhibits rotational and translational degrees of freedom in solutions or glasses. An ensemble of qubits with anisotropic **g** or **A** tensors can dephase through molecular rotations with respect to the applied magnetic field (Figure 4B), which alters the resonance frequency conditions and decreases T_M.[52] Due to the characteristic anisotropy of **g** and **A** in transition metal complexes, the T_M of transition-metal-based qubits is often more sensitive to orientation than that of organic radicals. Orientation-dependent T_M values for paramagnetic transition metal complexes in frozen solution have been attributed to small-angle librations (hindered rotations) at temperatures well below the glass-transition temperature of the frozen glasses. Such librations are not prevalent in crystals. Experimentally, strong T_M orientation dependence was observed for a Cr(V) tetratolyl-porphyin complex in the glassy state but not in crystals.[57] Orientation-dependent studies of T_M can therefore provide a selective diagnostic for librational decoherence processes. The role of the counterion structure in glasses has also been investigated. Through analyses of the temperature dependent T_M times, it was proposed that methyl rotors proximal to the electron spin have a detrimental impact

on T_M.[58] However, similar T_M behavior has also been observed in systems with no methyl groups present.[49]

The well-studied class of V(IV) qubits contain experimental examples in each of the three decoherence regimes, providing for an instructive conceptual comparison. The electron spin relaxation of vanadyl phthalocyanine (VOPc) has been studied in a glassy frozen solution,[59] a pure crystalline solid,[38] and diamagnetically diluted crystalline dispersions in titanyl phthalocyanine (TiOPc) host at 1:10, 1:100, and 1:1000 concentrations.[38,49] At 300 K in 1:10 dilution, VOPc exists in the spin-spin regime, where T_M is significantly smaller than T_1 owing to electronic dipolar contributions to decoherence. However, the 1:1000 dilution displays $T_M \sim T_1$ at 300 K, indicating T_M is T_1 limited.[38] The increased dilution suppresses dipolar interactions and causes phonon contributions to dominate decoherence, moving VOPc from the spin-spin regime to the spin-phonon regime through sample preparation. Finally, the V(IV) qubit $(n\text{-}Bu_3NH)_2[V(C_6H_4O_2)_3]$ in a frozen glass has demonstrated 20 % variation in T_M times as a function of field position, consistent with motional contributions to decoherence.[60] It is to be expected that other V(IV) qubits will demonstrate the same behavior. These examples show how sample preparation and measurement conditions can place a qubit into any one of the three decoherence regimes. Further research is needed to ascertain how spin-phonon contributions to decoherence change when a qubit moves from a crystalline to a motional environment, an effort which may prove key for applications in quantum sensing.

Crystal packing effects can also play a significant role in magnetic decoherence properties. A study comparing two different crystal packing modes of lanthanide-based nitroxide radicals showed that the structure with proximal intermolecular nitroxide spins possessed the stronger spin-spin exchange coupling.[61] Crystal packing thus modulates the strength of the spin-spin

decoherence regime for magnetically undiluted crystals. Further research is required to elucidate the effect of ligand spin polarization on decoherence.

Phonon Contributions to Decoherence

In the crystalline solid phase, thermodynamic spin relaxation transfers energy to lattice phonons. At high temperatures, this relaxation process causes T_M to become T_1-limited,[62] defining the spin-phonon regime of decoherence. Two criteria must hold for spin-phonon mediated relaxation processes.[63],[64] First, energy conservation must be satisfied, implying that only lattice processes matching the spin-flip energy can occur. This could arise through emission of a single phonon possessing the correct spin-flip energy (direct mechanism[16,65]), inelastic scattering of two phonons with the correct energy difference via a virtual state (Raman mechanism[16,65]), or two phonon relaxation through a real electronic excited state (Orbach mechanism[16,66]), as shown in Figure 5A. In dilute monometallic S = ½ qubits, contributions from the Orbach mechanism are often negligible owing to the lack of thermally accessible electronic excited states.[67] Second, there must be a nonzero transition probability for the energy to transfer from the spin to the lattice phonon, a criterion known as spin-phonon coupling. The theoretical underpinnings for spin-lattice relaxation in solids were developed by Van Vleck,[65,68] Pryce,[69] Orbach,[70] and others.[71,72]

Temperature Scaling

To diagnose the dominant phonon mechanism, early spin-phonon relaxation literature focused on deriving functional forms for how T_1 scales with temperature (T) and magnetic field (B). For example, treatment for S = ½ systems resulted in $1/T_1 \propto B^4T$ for the direct process and $1/T_1 \propto T^9$ and $1/T_1 \propto B^2T^7$ for the Raman process.[16] It is crucial to note, however, that these derivations use

10.1002/chem.202100845

the Debye model, which describes crystal vibrations solely as acoustic phonons (i.e. displacement waves, Figure 5B) carrying momentum and possessing a linear dispersion relation.[73] Optical phonons (Figure 5B), which include the intramolecular vibrations commonly analyzed in molecular vibrational spectroscopy, are not considered in the Debye model. This assumption has two key consequences for a spin-phonon coupling model:[63,65,74] (1) relaxation takes place exclusively through scattering of acoustic phonons rather than optical phonons, and (2) the spin-phonon coupling constants for each phonon mode are equal or follow some predictable functional form, as no provision can be made for unique spin-phonon coupling for distinct intramolecular vibrations.[63] For more details on spin-phonon implications of the Debye model, see the perspective by Coronado, Gaita-Ariño and coworkers.[75]

10.1002/chem.202100845

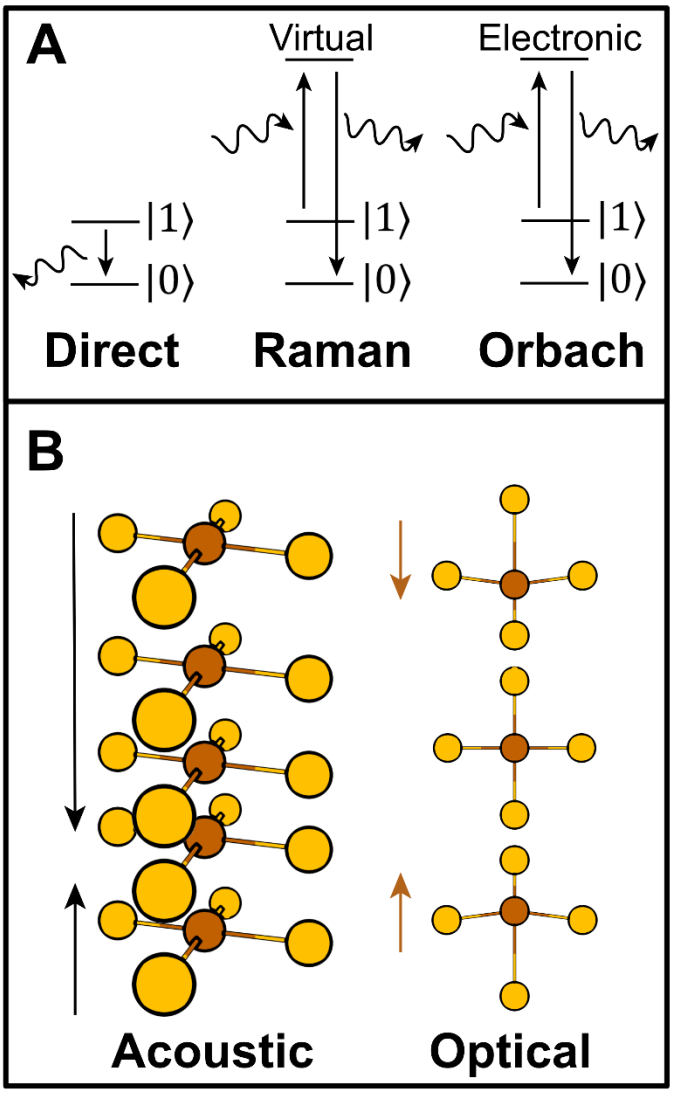

Figure 5. *Phonon involvement in spin-lattice relaxation.* ***(A)*** *Mechanisms of phonon-induced relaxation. Zig-zag arrows represent phonon scattering.* ***(B)*** *Schematics of the two types of phonons involved in relaxation processes in molecular solids. Acoustic phonons are characterized by displacement waves, while optical phonons additionally involve intramolecular vibrations.*

The temperature scaling relationships derived from the Debye model often show excellent agreement with experiment for homogeneous extended solids at low temperatures, such as Tm^{2+} in alkaline earth fluorides.[76] However, the Debye model assumptions are no longer appropriate

when localized molecular vibrations become thermally activated with increasing temperature. In an extended solid, such local modes may be attributed to defects in the crystal structure.[77],[78] In a molecular solid, local modes correspond to optical phonons with large intramolecular vibrational character (Figure 5B).[73,79] Models for the temperature scaling of Raman relaxation through local modes have produced several new functional forms,[77,78] including $1/T_1 \propto T^3$, $1/T_1 \propto T^5$, and $1/T_1 \propto \exp(T)/(\exp(T) - 1)^2$.

While useful as empirical tools for analyzing data, the proliferation of such functional forms points to the theoretical inability of the Debye model to describe the spin-phonon decoherence regime in molecular solids. In such materials, spin-lattice relaxation involves Raman processes with optical phonons, and the density of states for optical phonons is in general not homogeneous.[80,81] Furthermore, the spin-phonon coupling terms in molecular solids may vary by orders of magnitude depending on the phonon mode under consideration.[80,82] These effects are not captured in the Debye model temperature scaling predictions, rendering deviations from experiment unsurprising.[79,83] Distinctly molecular models of spin-lattice relaxation are thus required to understand the spin-phonon regime and pinpoint the specific vibrational modes that contribute to decoherence.

Coupling mechanisms

A second issue relates to the source of the spin-phonon coupling, which is a distinct consideration from the phonon mechanism (direct, Raman, Orbach). Coupling arises when phonons modulate the spin Hamiltonian; that is, $\partial \boldsymbol{H}_{spin}/\partial Q_i$ is nonzero for atomic displacements that take place along the vibrational coordinate Q_i of mode i.[64,82] For an S = ½ qubit (Equation 1), both the g-tensor ($\boldsymbol{g}$) and the hyperfine tensor ($\boldsymbol{A}$) can have significant nonzero derivatives with respect to

10.1002/chem.202100845

nuclear motion along Q_i. Assuming weak coupling, this yields two types of terms contributing to the spin-phonon interaction:[64,84]

$$\frac{\partial \boldsymbol{H}_{\boldsymbol{spin}}}{\partial Q_i} = \mu_e \boldsymbol{B_0} \cdot \frac{\partial \boldsymbol{g}}{\partial Q_i} \cdot \hat{\boldsymbol{S}} + \hat{\boldsymbol{S}} \cdot \frac{\partial \boldsymbol{A}}{\partial Q_i} \cdot \hat{\boldsymbol{I}} \quad (2)$$

Equation 2 gives first-order spin-phonon coupling terms for the direct process.[84] Mixed partial derivatives relate to the Raman process, but the magnitudes of the mixed partial derivatives are expected to trend similarly to the first derivatives.[80] Each phonon mode has unique spin-phonon coupling terms, which may be either zero or non-zero. Owing to larger modulations of the first coordination sphere of the spin bearing metal ion (Figure 5B), optical phonons exhibit much larger spin-phonon coupling terms than acoustic phonons.[64] Optical phonons therefore dominate spin-lattice relaxation when the temperature is high enough for their thermal population. Optical bands may be approximated by molecular vibrations at the gamma point (zero phonon momentum), enabling description of the Raman process solely through molecular quantities.[80] An active area of research seeks to understand the physical origins (i.e., molecular geometry and bonding) of the magnitudes of spin-phonon coupling coefficients under different experimental conditions.[64,82,85,86] For example, a recent study of the S = ½ organometallic [Cp(Ti)(cot)] complex found that it possesses a surprisingly long T_M, attributed to weak spin-phonon coupling with the d_{z^2} ground state.[87]

New Models

Two recent complementary approaches that go beyond the Debye model have gained new insights into relaxation in the spin-phonon regime. First, the *ab initio* spin dynamics approach of Lunghi, Sanvito, Sessoli, and coworkers seeks to computationally predict T_1 from the full phonon

dispersion relation, calculating the unique spin-phonon coupling contribution from each phonon mode across the entire Brillioun zone. The predicted temperature scalings for T_1 are a good match for available experimental data.[64,83,84] A key breakthrough in high temperature spin-lattice relaxation modeling was achieved by using machine learning to predict the $\boldsymbol{g}$ and $\boldsymbol{A}$ tensor values as a function of molecular geometry.[83,84] This made second-order numerical differentiation of the $\boldsymbol{g}$ and $\boldsymbol{A}$ tensors computationally tractable for the first time, enabling *ab initio* prediction of the Raman relaxation processes dominating at high temperature.[84] Additionally, four-dimensional inelastic neutron scattering was recently used to map the phonon dispersion of a transition metal qubit, providing an experimental calibration of the phonon states responsible for magnetic relaxation.[88] The *ab initio* spin dynamics approach rigorously considers all spin-phonon coupling coefficients, but places less emphasis on interpreting the electronic structure origins of the $\boldsymbol{g}$ and $\boldsymbol{A}$ tensor derivatives.

A second approach uses ligand field theory and molecular vibrations to understand the origins of the dynamic Hamiltonian tensor values.[82,89] This method provides a chemical explanation of the factors responsible for spin-phonon coupling, along with a mode-by-mode description of which molecular vibrations contribute the most to decoherence across different coordination geometries and electronic structures. Such a description enables targeted molecular design focused on specific vibrational modes rather than the unspecific "rigidity" descriptor of the Debye model.[75] The ligand field method is outlined in the following section.

Dynamic Ligand Fields in Electron Spin Qubits

The ground states of free transition metal ions have intrinsic in-state orbital angular momentum, as the degenerate set of d orbitals can freely rotate into one another with no energy barrier. The g

10.1002/chem.202100845

value in these cases can be predicted through the Landé formula and in general deviates strongly from the free-electron g value of 2.0023 (g_e). For example, a free Cu^{2+} ion with a ground state of $^2D_{5/2}$ has a predicted g value of 1.2. In the ligand fields encountered for molecular qubits, the ground state is orbitally nondegenerate, which quenches in-state orbital angular momentum. However, spin-orbit coupling between ground and excited states can reintroduce orbital angular momentum into the ground state (out-of-state orbital angular momentum). The impact on the g value from this orbital angular momentum can be expressed through the general perturbative expression for the g value of a given d electron ground state:[90]

$$g_i = g_e - 2\lambda \sum_{e \neq g} \frac{\langle \Psi_g | \hat{\boldsymbol{L}}_{\boldsymbol{i}} | \Psi_e \rangle \langle \Psi_e | \hat{\boldsymbol{L}}_{\boldsymbol{i}} | \Psi_g \rangle}{E_e} \quad (3)$$

Here Ψ_g and Ψ_e represent ground and excited state wavefunctions, respectively, E_e represents the energy of Ψ_e relative to the ground state, $\hat{\boldsymbol{L}}_{\boldsymbol{i}}$ is an orbital angular momentum operator, and λ is the many-electron spin-orbit coupling constant. Note $\lambda = \pm\zeta_{3d}/2S$, where S is the total electron spin, ζ_{3d} is the one-electron spin-orbit coupling constant, and + and – are used for less than half filled and greater than half filled d^n shells, respectively. Taking D_{4h} $[CuCl_4]^{2-}$ as an example, the g_z ($g_\parallel$) value is modified by spin-orbit coupling between the $^2B_{2g}$ (d_{xy}) excited state and the $^2B_{1g}$ ($d_{x^2-y^2}$) ground state. Table 1 gives the effect of $\hat{\boldsymbol{L}}_{\boldsymbol{i}}$ on real d orbitals and can be used in conjunction with Equation 3 to derive a simple formula for g_z, where a factor η is used to account for the covalencies of the donor and acceptor orbitals of the ground and excited states:[91]

$$g_z = g_e - 2\frac{\lambda\eta\langle x^2 - y^2 | \hat{\boldsymbol{L}}_{\boldsymbol{z}} | \mathrm{xy} \rangle \langle \mathrm{xy} | \hat{\boldsymbol{L}}_{\boldsymbol{z}} | x^2 - y^2 \rangle}{E_{B_{2g}}} = g_e - \frac{8\lambda\eta}{E_{B_{2g}}} \quad (4)$$

10.1002/chem.202100845

Table 1. Application of orbital angular momentum operators to the real d orbitals.

$\hat{L}_x$	$\hat{L}_y$	$\hat{L}_z$
$\hat{L}_x d_{xz} = -i d_{xy}$	$\hat{L}_y d_{xz} = i d_{x^2-y^2} - i\sqrt{3} d_{z^2}$	$\hat{L}_z d_{xz} = i d_{yz}$
$\hat{L}_x d_{yz} = i\sqrt{3} d_{z^2} + i d_{x^2-y^2}$	$\hat{L}_y d_{yz} = i d_{xy}$	$\hat{L}_z d_{yz} = -i d_{xz}$
$\hat{L}_x d_{xy} = i d_{xz}$	$\hat{L}_y d_{xy} = -i d_{yz}$	$\hat{L}_z d_{xy} = -2i d_{x^2-y^2}$
$\hat{L}_x d_{x^2-y^2} = -i d_{yz}$	$\hat{L}_y d_{x^2-y^2} = -i d_{xz}$	$\hat{L}_z d_{x^2-y^2} = 2i d_{xy}$
$\hat{L}_x d_{z^2} = -i\sqrt{3} d_{yz}$	$\hat{L}_y d_{z^2} = i\sqrt{3} d_{xz}$	$\hat{L}_z d_{z^2} = 0$

It should be noted that the η parameter can be derived from the spin densities of the metal ion and ligating atoms: a lower spin density on the metal center indicates a more covalent interaction, in which less spin on the metal is available to spin-orbit couple with d-d excited states. This proxy for covalency therefore takes into account the delocalization of spin density with the ligating environment. An important assumption here is that λ for the metal ion is much greater than that of the ligands, which justifies treating spin-orbit coupling only in the d-d manifold. The error in this approximation increases when heavy ligand atoms are present. However, contributions from ligand-based spin-orbit coupling may be incorporated into the model.

To minimize spin-phonon coupling, $\partial \boldsymbol{g}/\partial Q$ should be as small as possible (Equation 2). By differentiating Equation 4 with respect to the i^{th} vibrational coordinate, we obtain an analytical expression for the spin-phonon coupling coefficient for g_z:[82]

$$\frac{\partial g_z}{\partial Q_i} = 8\lambda \frac{\eta\left(\frac{\partial E_{B_{2g}}}{\partial Q_i}\right) - E_{B_{2g}}\left(\frac{\partial \eta}{\partial Q_i}\right)}{\left(E_{B_{2g}}\right)^2} \quad (5)$$

The logic behind the ligand field model of decoherence is summarized in Figure 6. As was previously shown, the spin-phonon coupling coefficients for a wide variety of molecular electron

10.1002/chem.202100845

spin qubits qualitatively track with increased T_M in the spin-phonon decoherence regime.[82] Crucially, Equation 5 expresses these coefficients in terms of spectroscopically observable and computationally accessible quantities: d-d ligand field transition energies ($E_{B_{2g}}$), ligand–metal covalencies (η), and the many-electron spin-orbit coupling constant of the metal ion (λ). The energies of ligand field excited states of first-row transition metal complexes can be quantified by a combination of electronic absorption[91] and magnetic circular dichroism (MCD) spectroscopies.[92] However, highly covalent ligand–metal bonds, which are often present in molecular qubit candidates, can lead to low-energy, high-intensity charge transfer transitions. These, together with intra-ligand molecular excited states with large dipole allowed intensities (e.g, Soret and Q-bands in porphyrins and phthalocyanines), can obscure ligand field transitions even when using low temperature MCD. X-ray spectroscopies provide powerful approaches to overcome these limitations by gaining metal-centric electronic structure insights in highly covalent systems. For example, the covalencies of ligand–metal bonds can be quantified using metal L-edge[93,94] and ligand K-edge[95] X-ray absorption spectroscopies. Additionally, 2p3d resonant inelastic X-ray scattering (RIXS) can be utilized to directly measure spin-allowed and spin-forbidden ligand field excited state energies.[96,97] 1s2p RIXS can also provide L-edge-like data using hard X-rays through constant incident energy (CIE) cuts taken within the 1s-3d K pre-edge.[98] Therefore, combining inorganic electronic spectroscopies with the dynamic ligand field model can provide a quantitative experimental basis for understanding bonding and electronic structure contributions to molecular qubit coherence times.

10.1002/chem.202100845

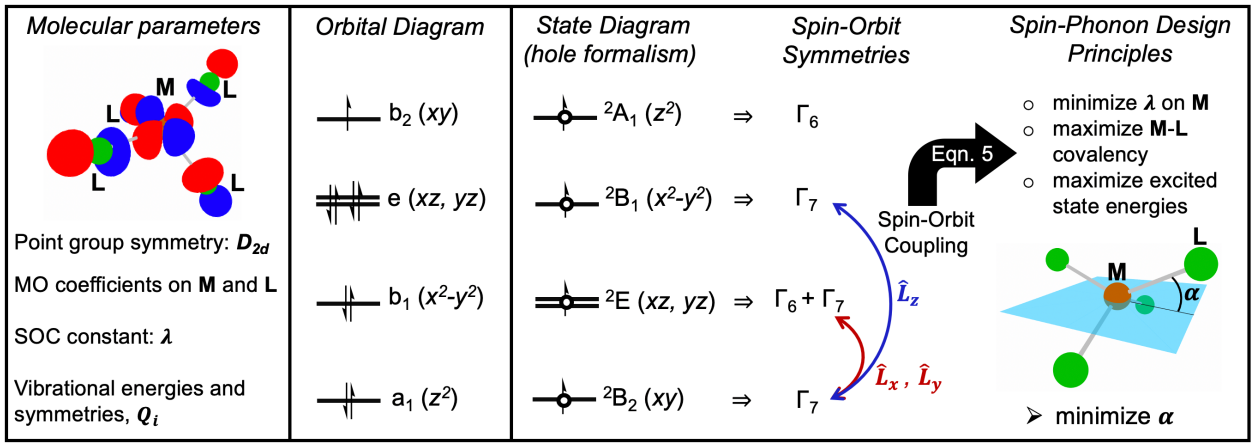

Figure 6. *A general ligand field theory method for predicting decoherence in the spin-phonon regime from equilibrium molecular parameters (example: D_{2d} d^9 ML_4 complex). A molecular orbital diagram containing metal d-based orbitals can be mapped to a state diagram, and spin-orbit coupling contributions can be evaluated using the corresponding double group (shown in Bethe notation) to obtain molecular g values. With the aid of Equation 5, minimization of $\partial \boldsymbol{g}/\partial Q$ for the lowest-energy bending mode can be achieved by obtaining a planar equilibrium geometry (see also Figure 7).*

Equation 5 suggests two approaches for engineering long coherence times in molecular electron spin qubits. First, the overall ground state orbital angular momentum can be minimized, as $\partial \boldsymbol{g}/\partial Q$ is lessened when $\boldsymbol{g}$ is small initially. This can occur by (1) decreasing the spin-orbit coupling constant, (2) increasing the excited state energy separation, (3) increasing the covalencies of ligand–metal bonds, or (4) engineering a ground state wave function that cannot engage in excited state spin-orbit coupling. Consideration of the d orbital rotations enables the latter strategy through direct evaluation of orbital angular momentum matrix elements for S = ½ qubits. As shown in Table 1, the d_{z^2} orbital cannot rotate into any other d orbital about the z-axis, so a molecule with a d_{z^2} ground state should exhibit small spin-phonon coupling with the g_z transition.

Experimentally, a yttrium complex with a partially covalent $4d_{z^2}/5s$-based ground state demonstrated a μs T_M at room temperature, despite featuring ligands with nuclear spins, unoptimized magnetic dilution, and a non-rigid ligand framework.[39] This example establishes minimizing ground state orbital angular momentum as a powerful design principle for engineering molecular qubits within the spin-phonon decoherence regime.

Second, the magnitude of the vibrational derivatives can be directly decreased by employing ligand frameworks with few vibrational modes that can undergo spin-phonon coupling.[48,82] This can be accomplished by either (1) reducing the vibrational density of states at low energies,[62] as thermal phonon occupation is required for the Raman relaxation process, or (2) tailoring the coordination geometry to reduce spin-phonon coupling by symmetry.[48] Dynamic ligand field analysis of a $[CuCl_4]^{2-}$ model compound has illuminated how vibrational symmetry can engender an optimal coordination geometry for S = ½ Cu(II) qubits.[82] Depending on the counterion, $[CuCl_4]^{2-}$ can adopt a square planar (D_{4h}) or distorted tetrahedral (D_{2d}) crystal geometry.[99] These two structures are directly related by a low-energy bending mode (Figure 7A). Analyses of the ground and excited state potential energy surfaces (PESs) along this coordinate provide insight into the electronic structure origins of spin-phonon coupling over different structures. For example, at the D_{4h} geometry, there is no excited state distortion and therefore no excited state linear coupling term (Figure 7B, dashed blue line). The absence of linear excited state coupling eliminates linear spin-phonon coupling in the ground state. For D_{2d}, however, the excited state PES is shifted relative to the ground state (i.e., there is an excited state distorting force), giving rise to a non-zero excited state linear coupling term for the D_{2d} structure. This provides a mechanism for the amount of orbital angular momentum mixed into the D_{2d} ground state to dynamically fluctuate along Q_i (Figure 7B-C). This analysis demonstrates that new vibrational

modes can be activated for spin-phonon coupling upon small modifications of the coordination geometry.[100–102]

Density functional theory (DFT) calculations confirm that the D_{4h} $[CuCl_4]^{2-}$ g_z value exhibits linear spin-phonon coupling along only the totally symmetric stretching mode (i.e., breathing mode). However, upon distorting to the D_{2d} geometry, the bending distortion mode changes in symmetry from b_{2u} (in D_{4h}) to a_1 (in D_{2d}), thus activating it for linear spin-phonon coupling (Figure 7F). The spin-phonon coupling (arrow size) clearly increases as the distortion angle α departs from 180° and the slope of the g_z surface (i.e., $\partial g_z/\partial Q_\alpha$) increases. At α = 180°, the surface flattens as linear spin-phonon coupling in the bending mode is removed. Examination of the covalency (Figure 7D) and excited state energies (Figure 7E) shows these quantities correlate strongly with the g_z value, as expected on the basis of Equations 4 and 5.[82] This model explains why Cu(II) transition metal complexes with the longest T_1 times host a square planar geometry around the metal center, while tetrahedrally distorted complexes exhibit shorter T_1 times.[79] While vibrational symmetry effects have so far been investigated in the context of discrete molecular qubits,[48] such strategies will likely also prove important in designing arrays of qubits in MOFs, where a large density of low-energy phonons leads to enhanced spin-phonon coupling.[45,46]

Notably, the gas phase equilibrium geometries of four-coordinate Cu(II) complexes are D_{2d}. However, ligand field strain through crystal packing effects can enforce geometries that would otherwise be out of equilibrium, similar to the concept of the entatic state in bioinorganic chemistry.[99,103] Cu complexes featuring symmetry- and distortion-altering intramolecular steric interactions have also been developed. These interactions can strongly influence ground state redox potentials and reorganization energies, as well as the lifetimes of metal-to-ligand charge

transfer excited states for Cu(I).[101,102,104] Similar ligand design approaches will enable systematic evaluation of how ligand field strain and secondary coordination sphere interactions contribute to coherence times Cu(II) qubit candidates.

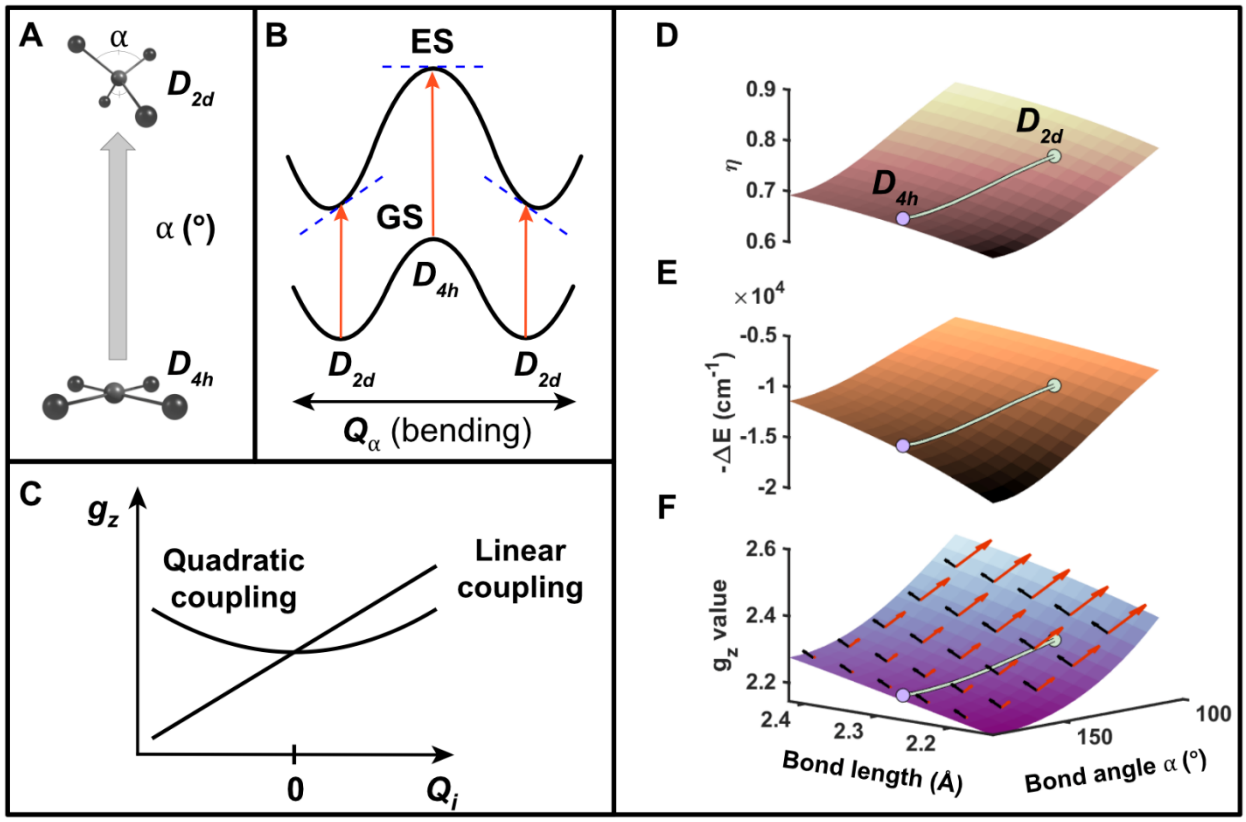

Figure 7. *Effect of geometric distortion on spin-phonon coupling terms.* ***(A)*** *D_{4h} and D_{2d} $[CuCl_4]^{2-}$ are related by a distortion parametrized by bond angle α.* ***(B)*** *The ground and excited state equilibrium geometry mismatch at D_{2d} leads to linear excited state coupling (dashed blue lines) for the bending mode.* ***(C)*** *Linear versus quadratic spin-phonon coupling.* ***(D)***, ***(E)***, ***(F)*** *represent the variation of Cu d orbital contribution, first excited state energy, and g_z in $[CuCl_4]^{2-}$ as a function of geometry, respectively. Arrows give the spin-phonon coupling terms along the symmetric stretch (black) and bending (red) modes. Adapted from Ref. 79.*

The interplay between factors in the dynamic ligand field model can be illustrated by recent studies comparing Cu(II) and V(IV) S = ½ qubit candidates.[49,62] It was experimentally shown that the T_1 of vanadyl phthalocyanine (VOPc) is longer than that of copper phthalocyanine (CuPc) at higher temperatures (>25 K) where the spin-phonon regime dominates,[49] with VOPc exhibiting coherence up to room temperature.[38] These results can be rationalized and quantitatively understood using the spin-phonon coupling factors found in Equation 5: (1) the energy of the ligand field excited state that spin-orbit couples with the ground state, (2) the covalencies of the ligand–metal bonds, and (3) the spin-orbit coupling constant. To the best of our knowledge, the specific ligand field transition contributions to the g values of CuPc and VOPc are not known experimentally, likely due to the intense, dominant intra-Pc contributions to the electronic absorption spectrum. For g_z, they were calculated to be similar in energy (22,165 and 22,745 cm^{-1}, respectively[82]), so (1) is likely not the distinguishing factor between CuPc and VOPc. Ligand–metal covalency in the ground state wave function is significantly larger in CuPc relative to VOPc, but this would suggest a longer coherence time for CuPc, so (2) is not the distinguishing factor. Thus, in the comparison between Cu(II) and V(IV)O in the same equatorial ligand set, the significantly reduced spin-orbit coupling constant of V(IV) in VOPc is of critical importance. Indeed, DFT calculations show that spin-phonon coupling coefficients between comparable vibrational modes of CuPc and VOPc differ primarily by the ratio of the spin-orbit coupling constants.[82]

In a comparison between four-coordinate $[Cu(II)(bdt)_2]^{2-}$ (bdt=benzene-1,2-dithiolate) and six-coordinate $[V(IV)(bdt)_3]^{2-}$, the observation of longer electron spin relaxation for the former was ascribed to increased covalency of the Cu(II)–S bonds. Interestingly, this is opposite of the behavior observed for CuPc vs VOPc, where longer coherence times were observed for the more

ionic ground state. While $[Cu(bdt)_2]^{2-}$ is square planar, $[V(bdt)_3]^{2-}$ adopts a pseudo-octahedral coordination geometry and was calculated to have seventeen linear spin-phonon coupling active vibrational modes below 400 cm^{-1} for g_z; square planar $[Cu(bdt)_2]^{2-}$ has only one for g_z.[82] Additionally, lower energy excited states in the six-coordinate V(IV) complexes, which increase ground state orbital angular momentum and thus sensitivity to spin-phonon coupling, may also be of critical importance for determining relaxation times. Thus, based on the ligand field theory model, the shorter coherence time in the six-coordinate V(IV) complex arises from increased spin-phonon coupling relative to the Cu(II) complex due to the different coordination environment, despite the lower spin-orbit coupling constant of the former. While substitution of sulfur with selenium in the ligands (forming benzene-1,2-diselenate, bds) increases the ligand–metal covalency, T_1 values were experimentally observed to decrease for both Cu(II) and V(IV). This likely arises because the heavy atom substitution decreases the frequency of the spin-phonon coupling active vibrational modes, thereby increasing the thermal population and total spin-phonon coupling, even though the spin-phonon coupling coefficient itself may decrease due to increased covalency.[62,82] An additional factor to consider is the significantly increased spin-orbit coupling constant of selenium relative to sulfur, which will also contribute to accelerated relaxation. The considerations in this Section demonstrate the critical importance of evaluating dynamic ligand field properties when comparing coherence times between different molecular qubit candidates, especially if they feature different first coordination spheres.

The ligand field model of spin-phonon coupling as described is general for understanding couplings in any S = ½ system. It has also been adapted for studying S > ½ systems. Here modulation of **D** and **E** in the zero-field splitting Hamiltonian along vibrational coordinates enables a description of excited state intersystem crossing and single molecule magnet relaxation.[105]

Further extensions of the ligand field model are possible to also account for hyperfine contributions[64] ($\partial \boldsymbol{A}/\partial Q$) to spin-lattice relaxation.

Summary and Outlook

The study of electron spin relaxation has a rich history and much is known. However, further understanding decoherence mechanisms at the molecular level is a key step towards the development of quantum technologies that can employ the versatility and tunability of coordination complexes. Here we have leveraged the idea of coherence regimes to highlight specific molecular contributions to decoherence. It is clear that the conditions (temperature, solid/solution phase) of the desired quantum application (computing/sensing) will define the specific design principles. In the spin-spin decoherence regime, decreasing spin-spin interactions through magnetic dilution and decreasing the concentration or gyromagnetic ratios of nuclear spins has the largest impact on prolonging T_M. In the motional regime, molecular tumbling and librational dynamics alter the resonance frequency conditions and decrease T_M. At higher temperatures in the solid state, T_M is limited by T_1. We find this spin-phonon regime particularly exciting, as it provides a means for fundamental studies of how specific atomic motions are coupled to dynamic electronic structure changes. These considerations are also crucial for understanding time-dependent magnetization phenomena beyond quantum information science, including single-molecule magnetism, spin crossover complexes, and the kinetics of photomagnetic processes. From considering dynamic ligand fields, several strategies for minimizing spin-phonon coupling have been characterized and applied to experimental case studies. It is important to note, however, that the specific molecular vibration(s) that are responsible for decoherence in the spin-phonon regime have yet to be experimentally assigned. In

the future, we anticipate that the dynamic ligand field model will provide an analytical link between molecular vibrations and temperature dependent electron spin relaxation rates. This will facilitate experimental assignment of the decoherence-inducing vibrations, allowing for a more tailored synthetic design approach to prolonging T_M.

Careful examination of the various decoherence mechanisms also provides insights into applications beyond quantum computing. These considerations extend nicely to the development of qubits as molecular quantum sensors (qusors), which provide several attractive features: (1) the ability to target local regions of space on a molecular level, (2) novel coherence-based sensing mechanisms, and (3) a platform for fundamental studies of coherence in chemical microenvironments formed on electrode interfaces or in biological systems. In solution phases, including cases where qusors are immobilized on surfaces or bound to larger macromolecular structures (e.g., proteins), the magnitude of motional contributions to decoherence will be important to consider. By tailoring the ground state orbital angular momentum anisotropy and the molecular vibrations, it will be possible to design qusors that selectively sense rotational versus vibrational degrees of freedom and vice-versa, providing new insight into molecular dynamics in chemical microenvironments. Ligand sets with peripheral H-bond donors and acceptors may also provide a strategy to "lock-in" a specific molecular orientation and limit motional contributions. Additionally, it may be possible to sense the local electric fields in chemical microenvironments through their effects on T_1 and T_M, lending insight into the functional role of the local electrostatic environment. Previous work by Mims has shown that electron spin precession can be perturbed by an external electric field.[106] Electric field sensing has already been accomplished using solid state systems such as nitrogen vacancies in diamond,[9,107] but solid state sensors have inherently limited spatial resolution and tunability. An exciting molecular engineering challenge will be to tune and

enhance qusor electric field sensitivity through noncentrosymmetric perturbations manifesting in odd parity ligand field components,[106] while still minimizing spin-phonon coupling. This level of detailed understanding will derive from incorporating electric field effects into the dynamic ligand field model and learning to describe and control vibrational symmetry, which remains an outstanding challenge in engineering molecular electron spin qubits.

While many approaches to prolonging coherence times have sought to make qubit frameworks more rigid, there are a variety of important geometric and electronic structure factors that are not captured by this description. Detailed ligand field analyses coupled to high-resolution inorganic spectroscopies are called for to understand the role of molecular "rigidity" and symmetry by defining the precise vibrational modes that contribute to spin-phonon coupling and tuning their frequencies through synthetic design strategies. This level of new molecular insight will guide fundamental studies of spin-phonon coupling over a broad range of one-, two-, and three-dimensional S = ½ systems, as well as the development of electron spin qubit and qusor constructs for use in quantum technologies.

Acknowledgments

NPK acknowledges support by the National Science Foundation Graduate Research Fellowship under Grant No. DGE-1745301. Financial support from Caltech and the Dow Next Generation Educator Fund is gratefully acknowledged.

References

[1] J. P. Dowling, G. J. Milburn, *Philos. Trans. Math. Phys. Eng. Sci.* **2003**, *361*, 1655–1674.

[2] M. R. Wasielewski, M. D. E. Forbes, N. L. Frank, K. Kowalski, G. D. Scholes, J. Yuen-Zhou, M. A. Baldo, D. E. Freedman, R. H. Goldsmith, T. Goodson, M. L. Kirk, J. K. McCusker, J. P. Ogilvie, D. A. Shultz, S. Stoll, K. B. Whaley, *Nat. Rev. Chem.* **2020**, *4*, 490–504.

[3] M. A. Nielsen, I. L. Chuang, *Quantum Computation and Quantum Information: 10th Anniversary Edition*, Cambridge University Press, Cambridge, **2010**.
[4] A. Schweiger, G. Jeschke, *Principles of Pulse Electron Paramagnetic Resonance*, Oxford University Press, Oxford, UK ; New York, **2001**.
[5] I. Cimatti, L. Bondì, G. Serrano, L. Malavolti, B. Cortigiani, E. Velez-Fort, D. Betto, A. Ouerghi, N. B. Brookes, S. Loth, M. Mannini, F. Totti, R. Sessoli, *Nanoscale Horiz.* **2019**, *4*, 1202–1210.
[6] S. Cardona-Serra, A. Gaita-Ariño, *Dalton Trans.* **2018**, *47*, 5533–5537.
[7] A. Urtizberea, E. Natividad, P. J. Alonso, L. Pérez-Martínez, M. A. Andrés, I. Gascón, I. Gimeno, F. Luis, O. Roubeau, *Mater. Horiz.* **2020**, *7*, 885–897.
[8] C. Bonizzoni, A. Ghirri, M. Atzori, L. Sorace, R. Sessoli, M. Affronte, *Sci. Rep.* **2017**, *7*, 13096.
[9] F. Dolde, H. Fedder, M. W. Doherty, T. Nöbauer, F. Rempp, G. Balasubramanian, T. Wolf, F. Reinhard, L. C. L. Hollenberg, F. Jelezko, J. Wrachtrup, *Nat. Phys.* **2011**, *7*, 459–463.
[10] G. Kucsko, P. C. Maurer, N. Y. Yao, M. Kubo, H. J. Noh, P. K. Lo, H. Park, M. D. Lukin, *Nature* **2013**, *500*, 54–58.
[11] H. J. Mamin, M. Kim, M. H. Sherwood, C. T. Rettner, K. Ohno, D. D. Awschalom, D. Rugar, *Science* **2013**, *339*, 557–560.
[12] B. Hensen, H. Bernien, A. E. Dréau, A. Reiserer, N. Kalb, M. S. Blok, J. Ruitenberg, R. F. L. Vermeulen, R. N. Schouten, C. Abellán, W. Amaya, V. Pruneri, M. W. Mitchell, M. Markham, D. J. Twitchen, D. Elkouss, S. Wehner, T. H. Taminiau, R. Hanson, *Nature* **2015**, *526*, 682–686.
[13] Y. Yu, F. Ma, X.-Y. Luo, B. Jing, P.-F. Sun, R.-Z. Fang, C.-W. Yang, H. Liu, M.-Y. Zheng, X.-P. Xie, W.-J. Zhang, L.-X. You, Z. Wang, T.-Y. Chen, Q. Zhang, X.-H. Bao, J.-W. Pan, *Nature* **2020**, *578*, 240–245.
[14] M. H. Abobeih, J. Randall, C. E. Bradley, H. P. Bartling, M. A. Bakker, M. J. Degen, M. Markham, D. J. Twitchen, T. H. Taminiau, *Nature* **2019**, *576*, 411–415.
[15] M. J. Graham, J. M. Zadrozny, M. S. Fataftah, D. E. Freedman, *Chem. Mater.* **2017**, *29*, 1885–1897.
[16] K. J. Standley, R. A. Vaughan, *Electron Spin Relaxation Phenomena in Solids*, Springer US, Boston, MA, **1969**.
[17] D. P. DiVincenzo, *Fortschritte Phys.* **2000**, *48*, 771–783.
[18] F. Bloch, *Phys. Rev.* **1946**, *70*, 460–474.
[19] V. V. Kurshev, A. M. Raitsimring, *J. Magn. Reson. 1969* **1990**, *88*, 126–129.
[20] W. M. Witzel, S. D. Sarma, *Phys. Rev. Lett.* **2007**, *98*, 077601.
[21] J. J. L. Morton, A. M. Tyryshkin, R. M. Brown, S. Shankar, B. W. Lovett, A. Ardavan, T. Schenkel, E. E. Haller, J. W. Ager, S. A. Lyon, *Nature* **2008**, *455*, 1085–1088.
[22] H. Bluhm, S. Foletti, I. Neder, M. Rudner, D. Mahalu, V. Umansky, A. Yacoby, *Nat. Phys.* **2011**, *7*, 109–113.
[23] H.-P. Breuer, F. Petruccione, *The Theory of Open Quantum Systems*, Oxford University Press, Oxford, **2007**.
[24] K. Bader, D. Dengler, S. Lenz, B. Endeward, S.-D. Jiang, P. Neugebauer, J. van Slageren, *Nat. Commun.* **2014**, *5*, 5304.

[25] M. J. Graham, J. M. Zadrozny, M. Shiddiq, J. S. Anderson, M. S. Fataftah, S. Hill, D. E. Freedman, *J. Am. Chem. Soc.* **2014**, *136*, 7623–7626.
[26] C.-J. Yu, M. J. Graham, J. M. Zadrozny, J. Niklas, M. D. Krzyaniak, M. R. Wasielewski, O. G. Poluektov, D. E. Freedman, *J. Am. Chem. Soc.* **2016**, *138*, 14678–14685.
[27] M. J. Graham, M. D. Krzyaniak, M. R. Wasielewski, D. E. Freedman, *Inorg. Chem.* **2017**, *56*, 8106–8113.
[28] J. M. Zadrozny, J. Niklas, O. G. Poluektov, D. E. Freedman, *ACS Cent. Sci.* **2015**, *1*, 488–492.
[29] A. Ardavan, O. Rival, J. J. L. Morton, S. J. Blundell, A. M. Tyryshkin, G. A. Timco, R. E. P. Winpenny, *Phys. Rev. Lett.* **2007**, *98*, 057201.
[30] K. Bader, S. H. Schlindwein, D. Gudat, J. van Slageren, *Phys. Chem. Chem. Phys.* **2017**, *19*, 2525–2529.
[31] C. E. Jackson, C.-Y. Lin, S. H. Johnson, J. van Tol, J. M. Zadrozny, *Chem. Sci.* **2019**, *10*, 8447–8454.
[32] M. Shiddiq, D. Komijani, Y. Duan, A. Gaita-Ariño, E. Coronado, S. Hill, *Nature* **2016**, *531*, 348–351.
[33] S. Ghosh, S. Datta, L. Friend, S. Cardona-Serra, A. Gaita-Ariño, E. Coronado, S. Hill, *Dalton Trans.* **2012**, *41*, 13697–13704.
[34] J. M. Zadrozny, A. T. Gallagher, T. D. Harris, D. E. Freedman, *J. Am. Chem. Soc.* **2017**, *139*, 7089–7094.
[35] S. Giménez-Santamarina, S. Cardona-Serra, J. M. Clemente-Juan, A. Gaita-Ariño, E. Coronado, *Chem. Sci.* **2020**, *11*, 10718–10728.
[36] M. Atzori, S. Benci, E. Morra, L. Tesi, M. Chiesa, R. Torre, L. Sorace, R. Sessoli, *Inorg. Chem.* **2018**, *57*, 731–740.
[37] M. Atzori, E. Morra, L. Tesi, A. Albino, M. Chiesa, L. Sorace, R. Sessoli, *J. Am. Chem. Soc.* **2016**, *138*, 11234–11244.
[38] M. Atzori, L. Tesi, E. Morra, M. Chiesa, L. Sorace, R. Sessoli, *J. Am. Chem. Soc.* **2016**, *138*, 2154–2157.
[39] A.-M. Ariciu, D. H. Woen, D. N. Huh, L. E. Nodaraki, A. K. Kostopoulos, C. A. P. Goodwin, N. F. Chilton, E. J. L. McInnes, R. E. P. Winpenny, W. J. Evans, F. Tuna, *Nat. Commun.* **2019**, *10*, 1–8.
[40] S. L. Bayliss, D. W. Laorenza, P. J. Mintun, B. D. Kovos, D. E. Freedman, D. D. Awschalom, *Science* **2020**, *370*, 1309–1312.
[41] M. S. Fataftah, D. E. Freedman, *Chem. Commun.* **2018**, *54*, 13773–13781.
[42] N. Bar-Gill, L. M. Pham, A. Jarmola, D. Budker, R. L. Walsworth, *Nat. Commun.* **2013**, *4*, 1743.
[43] M. Warner, S. Din, I. S. Tupitsyn, G. W. Morley, A. M. Stoneham, J. A. Gardener, Z. Wu, A. J. Fisher, S. Heutz, C. W. M. Kay, G. Aeppli, *Nature* **2013**, *503*, 504–508.
[44] W. F. Koehl, B. B. Buckley, F. J. Heremans, G. Calusine, D. D. Awschalom, *Nature* **2011**, *479*, 84–87.
[45] C.-J. Yu, M. D. Krzyaniak, M. S. Fataftah, M. R. Wasielewski, D. E. Freedman, *Chem. Sci.* **2019**, *10*, 1702–1708.
[46] C.-J. Yu, S. von Kugelgen, M. D. Krzyaniak, W. Ji, W. R. Dichtel, M. R. Wasielewski, D. E. Freedman, *Chem. Mater.* **2020**, *32*, 10200–10206.

[47] J. R. Klauder, P. W. Anderson, *Phys. Rev.* **1962**, *125*, 912–932.
[48] F. Santanni, A. Albino, M. Atzori, D. Ranieri, E. Salvadori, M. Chiesa, A. Lunghi, A. Bencini, L. Sorace, F. Totti, R. Sessoli, *Inorg. Chem.* **2021**, *60*, 140–151.
[49] A. H. Follmer, R. D. Ribson, P. H. Oyala, G. Y. Chen, R. G. Hadt, *J. Phys. Chem. A* **2020**, *124*, 9252–9260.
[50] L. L. Wald, E. L. Hahn, M. Lukac, *J Opt Soc Am B* **1992**, *9*, 789–793.
[51] N. Bloembergen, *Physica* **1949**, *15*, 386–426.
[52] S. S. Eaton, G. R. Eaton, in *Distance Meas. Biol. Syst. EPR* (Eds.: L.J. Berliner, G.R. Eaton, S.S. Eaton), Springer US, Boston, MA, **2000**, pp. 1–27.
[53] M. J. Graham, C.-J. Yu, M. D. Krzyaniak, M. R. Wasielewski, D. E. Freedman, *J. Am. Chem. Soc.* **2017**, *139*, 3196–3201.
[54] A. D. Milov, K. M. Salikhov, Y. D. Tsvetkov, *Fiz. Tverd. Tela* **1973**, *15*, 1187–1195.
[55] A. Zecevic, G. R. Eaton, S. S. Eaton, M. Lindgren, *Mol. Phys.* **1998**, *95*, 1255–1263.
[56] E. R. Canarie, S. M. Jahn, S. Stoll, *J. Phys. Chem. Lett.* **2020**, *11*, 3396–3400.
[57] R. Konda, J.-L. Du, S. S. Eaton, G. R. Eaton, *Appl. Magn. Reson.* **1994**, *7*, 185–193.
[58] C.-Y. Lin, T. Ngendahimana, G. R. Eaton, S. S. Eaton, J. M. Zadrozny, *Chem. Sci.* **2019**, *10*, 548–555.
[59] K. Bader, M. Winkler, J. van Slageren, *Chem. Commun.* **2016**, *52*, 3623–3626.
[60] C. E. Jackson, C.-Y. Lin, J. van Tol, J. M. Zadrozny, *Chem. Phys. Lett.* **2020**, *739*, 137034.
[61] F. Pointillart, K. Bernot, G. Poneti, R. Sessoli, *Inorg. Chem.* **2012**, *51*, 12218–12229.
[62] M. S. Fataftah, M. D. Krzyaniak, B. Vlaisavljevich, M. R. Wasielewski, J. M. Zadrozny, D. E. Freedman, *Chem. Sci.* **2019**, *10*, 6707–6714.
[63] D. Gatteschi, R. Sessoli, J. Villain, *Molecular Nanomagnets*, Oxford University Press, Oxford, **2006**.
[64] A. Lunghi, S. Sanvito, *Sci. Adv.* **2019**, *5*, eaax7163.
[65] J. H. Van Vleck, *Phys. Rev.* **1940**, *57*, 426–447.
[66] R. Orbach, *Proc. R. Soc. Lond. A* **1961**, *264*, 458–484.
[67] Y. Zhou, B. E. Bowler, G. R. Eaton, S. S. Eaton, *J. Magn. Reson.* **1999**, *139*, 165–174.
[68] J. H. Van Vleck, *Phys. Rev.* **1941**, *59*, 724–729.
[69] M. H. L. Pryce, K. W. H. Stevens, *Proc. Phys. Soc. Sect. A* **1950**, *63*, 36–51.
[70] R. Orbach, *Proc. Phys. Soc.* **1961**, *77*, 821–826.
[71] A. Abragam, *The Principles of Nuclear Magnetism*, Clarendon Press, London, **1961**.
[72] K. W. H. Stevens, *Rep. Prog. Phys.* **1967**, *30*, 189–226.
[73] L. Gu, R. Wu, *Phys. Rev. B* **2021**, *103*, 014401.
[74] H. B. G. Casimir, F. K. du Pré, *Physica* **1938**, *5*, 507–511.
[75] L. Escalera-Moreno, J. J. Baldoví, A. Gaita-Ariño, E. Coronado, *Chem. Sci.* **2018**, *9*, 3265–3275.
[76] E. S. Sabisky, C. H. Anderson, *Phys. Rev. B* **1970**, *1*, 2028–2040.
[77] J. G. Castle, D. W. Feldman, P. G. Klemens, R. A. Weeks, *Phys. Rev.* **1963**, *130*, 577–588.
[78] J. G. Castle, D. W. Feldman, *Phys. Rev.* **1965**, *137*, A671–A673.
[79] A. J. Fielding, S. Fox, G. L. Millhauser, M. Chattopadhyay, P. M. H. Kroneck, G. Fritz, G. R. Eaton, S. S. Eaton, *J. Magn. Reson.* **2006**, *179*, 92–104.
[80] A. Albino, S. Benci, L. Tesi, M. Atzori, R. Torre, S. Sanvito, R. Sessoli, A. Lunghi, *Inorg. Chem.* **2019**, *58*, 10260–10268.

[81] L. Tesi, A. Lunghi, M. Atzori, E. Lucaccini, L. Sorace, F. Totti, R. Sessoli, *Dalton Trans.* **2016**, *45*, 16635–16643.
[82] R. Mirzoyan, R. G. Hadt, *Phys. Chem. Chem. Phys.* **2020**, *22*, 11249–11265.
[83] A. Lunghi, S. Sanvito, *J. Chem. Phys.* **2020**, *153*, 174113.
[84] A. Lunghi, S. Sanvito, *J. Phys. Chem. Lett.* **2020**, *11*, 6273–6278.
[85] L. Escalera-Moreno, N. Suaud, A. Gaita-Ariño, E. Coronado, *J. Phys. Chem. Lett.* **2017**, *8*, 1695–1700.
[86] M. Atzori, L. Tesi, S. Benci, A. Lunghi, R. Righini, A. Taschin, R. Torre, L. Sorace, R. Sessoli, *J. Am. Chem. Soc.* **2017**, *139*, 4338–4341.
[87] L. C. de Camargo, M. Briganti, F. S. Santana, D. Stinghen, R. R. Ribeiro, G. G. Nunes, J. F. Soares, E. Salvadori, M. Chiesa, S. Benci, R. Torre, L. Sorace, F. Totti, R. Sessoli, *Angew. Chem.* **2021**, *133*, 2620–2625.
[88] E. Garlatti, L. Tesi, A. Lunghi, M. Atzori, D. J. Voneshen, P. Santini, S. Sanvito, T. Guidi, R. Sessoli, S. Carretta, *Nat. Commun.* **2020**, *11*, 1751.
[89] A. Lunghi, *ArXiv191204545 Cond-Mat Physicsquant-Ph* **2019**.
[90] C. J. Ballhausen, *Introduction to Ligand Field Theory*, McGraw-Hill, **1962**.
[91] E. I. Solomon, *Comments Inorg. Chem.* **1984**, *3*, 227–320.
[92] E. G. Pavel, E. I. Solomon, in *Spectrosc. Methods Bioinorg. Chem.* (Eds.: E.I. Solomon, K.O. Hodgson), American Chemical Society, Washington, DC, **1998**, pp. 119–135.
[93] S. J. George, M. D. Lowery, E. I. Solomon, S. P. Cramer, *J. Am. Chem. Soc.* **1993**, *115*, 2968–2969.
[94] E. C. Wasinger, F. M. F. de Groot, B. Hedman, K. O. Hodgson, E. I. Solomon, *J. Am. Chem. Soc.* **2003**, *125*, 12894–12906.
[95] T. Glaser, B. Hedman, K. O. Hodgson, E. I. Solomon, *Acc. Chem. Res.* **2000**, *33*, 859–868.
[96] B. E. Van Kuiken, A. W. Hahn, D. Maganas, S. DeBeer, *Inorg. Chem.* **2016**, *55*, 11497–11501.
[97] M. M. van Schooneveld, R. W. Gosselink, T. M. Eggenhuisen, M. Al Samarai, C. Monney, K. J. Zhou, T. Schmitt, F. M. F. de Groot, *Angew. Chem. Int. Ed.* **2013**, *52*, 1170–1174; *Angew. Chem.* **2013**, *125*, 1208-1212.
[98] M. Lundberg, T. Kroll, S. DeBeer, U. Bergmann, S. A. Wilson, P. Glatzel, D. Nordlund, B. Hedman, K. O. Hodgson, E. I. Solomon, *J. Am. Chem. Soc.* **2013**, *135*, 17121–17134.
[99] R. K. Szilagyi, M. Metz, E. I. Solomon, *J. Phys. Chem. A* **2002**, *106*, 2994–3007.
[100] D. V. Scaltrito, D. W. Thompson, J. A. O'Callaghan, G. J. Meyer, *Coord. Chem. Rev.* **2000**, *208*, 243–266.
[101] M. W. Mara, K. A. Fransted, L. X. Chen, *Coord. Chem. Rev.* **2015**, *282–283*, 2–18.
[102] G. D. Stroscio, R. D. Ribson, R. G. Hadt, *Inorg. Chem.* **2019**, *58*, 16800–16817.
[103] E. I. Solomon, R. G. Hadt, *Coord. Chem. Rev.* **2011**, *255*, 774–789.
[104] T. Tsukuda, A. Nakamura, T. Arai, T. Tsubomura, *Bull. Chem. Soc. Jpn.* **2006**, *79*, 288–290.
[105] N. J. Higdon, A. T. Barth, P. T. Kozlowski, R. G. Hadt, *J. Chem. Phys.* **2020**, *152*, 204306.
[106] W. B. Mims, *The Linear Electric Field Effect in Paramagnetic Resonance*, Clarendon Press, Oxford, **1976**.
[107] T. Fujisaku, R. Tanabe, S. Onoda, R. Kubota, T. F. Segawa, F. T.-K. So, T. Ohshima, I. Hamachi, M. Shirakawa, R. Igarashi, *ACS Nano* **2019**, *13*, 11726–11732.

10.1002/chem.202100845

Table of Contents Graphic and Text

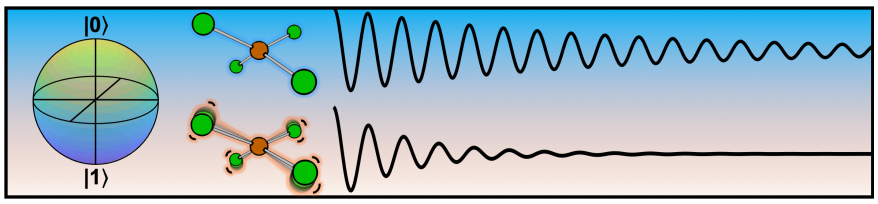

Controlling quantum decoherence in paramagnetic transition metal complexes enables the realization of next-generation quantum technologies from computing to sensing. Phenomena contributing to electron spin decoherence are deconstructed into three groups: the spin-spin, motional and spin-phonon regimes. Corresponding molecular design principles are described for each regime, with particular emphasis on the use of dynamic ligand field theory to analyze intramolecular vibrational contributions to decoherence.

Keywords: decoherence, electronic structure, ligand field theory, magnetic properties, qubit

10.1002/chem.202100845

Biographical Information

Ruben Mirzoyan

Ruben Mirzoyan received his H.B.Sc. degree in chemistry from the University of Toronto, Canada in 2018. Prior to graduate school, he worked with Profs. Gino G. Lavoie, Douglas W. Stephan, Pierre Kennepohl, Al-Amin Dhirani, and Gilbert C. Walker on topics ranging from organometallic catalysis to polaritonics in 2D materials. He is currently pursuing his Ph.D. at the California Institute of Technology in the group of Prof. Ryan G. Hadt, where he is interested in spin dynamics, materials for energy conversion and computational modeling of chemical systems.

10.1002/chem.202100845

Nathanael P. Kazmierczak

Nathanael P. Kazmierczak received his B.S. degree in chemistry from Calvin University, Grand Rapids, USA in 2020, where he worked in the lab of Prof. Douglas A. Vander Griend. From 2019-2020, he additionally worked as a visiting researcher in the lab of Prof. Kwabena Bediako at the University of California, Berkeley, USA. He is currently pursuing his Ph.D. degree in inorganic chemistry at the California Institute of Technology under the supervision of Prof. Ryan G. Hadt. His research interests include spin-phonon coupling, quantum sensing, two-dimensional materials, and chemical reaction network theory.

10.1002/chem.202100845

Ryan G. Hadt

Prof. Ryan G. Hadt received his B.S. and M.S. degrees in chemistry at the University of Minnesota Duluth (with V. N. Nemykin) and his Ph.D. at Stanford University (with E. I. Solomon). He was a visiting postdoctoral fellow at Harvard University (with D. G. Nocera) before continuing research at Argonne National Laboratory as a postdoctoral appointee (with L. X. Chen) and later as an Enrico Fermi Fellow. In 2018, he joined the faculty in the Division of Chemistry and Chemical Engineering at the California Institute of Technology. Prof. Hadt's research interests are broadly based in the fundamental understanding of transition metal electronic structure, with applications in catalysis, photophysics, and quantum information science.